Influence of dopants Ti and Ni on bonding interactions and dehydrogenation properties of lithium alanate

Y. Song,*[a] J. H. Dai,[a] X. M. Liang[a] and R. Yang[b]

Received 21st October 2009, Accepted 12th June 2010
DOI: 10.1039/b921924b

We report a study of the influence of Ti and Ni dopants on the stability and bonding interactions of $LiAlH_4$ using the first-principles method. Both the Ti and the Ni prefer to occupy an interstitial site in the $LiAlH_4$ owing to lower occupation energies estimated from the total energy calculations. Calculations show that the bonding interactions between the Al and the H atoms within the $[AlH_4]$ groups were significantly reduced by the dopants, and both the stability and the geometry of the $[AlH_4]$ group were distorted in the doped $LiAlH_4$ systems. However, Ti and Ni use different mechanisms to improve the dehydrogenation properties of $LiAlH_4$. The Ti dopant tends to interact with the Al atom in its neighbouring $[AlH_4]$ to 'free' the H atoms from these $[AlH_4]$ groups. The effect of Ni dopant on the stability and the bonding interactions of the $LiAlH_4$ is due to the induction of the Ni d electrons that could cause a bonding interaction between the Ni and the Al atoms, strengthening the interactions between the Li and the H atoms, and 'freeing' the H atoms from the neighbouring $[AlH_4]$ groups as well.

Introduction

A cornerstone of the hydrogen economy is vehicles powered by compact, lightweight and inexpensive hydrogen fuel cell systems. One of the key challenges of using hydrogen in mobile applications is the poor volumetric energy density of conventional hydrogen storage media. Solid-state storage of hydrogen in metal or complex hydrides offers enhanced volumetric hydrogen densities, but these media generally either have poor gravimetric capacity (<4 wt%) due to the additional weight of the host or release hydrogen at an impractically high temperature (>600 K). A class of metastable hydrides offers some new hope with high volumetric (>80 g of H_2/L) and gravimetric (≥ 8 wt%) energy densities and low decomposition temperature (<423 K), such as the lithium and magnesium alanate,[1,2] bialkalimetallic alanates,[3] and so on. However, these materials typically have very high dehydrogenation pressures (>1 kbar), and the organometallic reactions from which they are usually prepared are costly.

$LiAlH_4$ is one of the most promising candidates. Since the discovery of the improvability to the hydrogenation/dehydrogenation kinetics of the Ti catalyzed $NaAlH_4$,[4] the number of investigations into the suitability of $LiAlH_4$ as a H-storage material have greatly increased. It has been reported that $LiAlH_4$ is easily transformed into Li_3AlH_6, Al, and H_2 in the presence of catalysts or after prolonged ball-milling at room temperature by the following three steps:[5–11]

$$LiAlH_4 \rightarrow \tfrac{1}{3}Li_3AlH_6 + \tfrac{2}{3}Al + H_2 \quad (1)$$

$$Li_3AlH_6 \rightarrow 3LiH + Al + \tfrac{3}{2}H_2 \quad (2)$$

$$LiH + Al \rightarrow LiAl + \tfrac{1}{2}H_2 \quad (3)$$

The first and second reactions released 5.3 wt% and 2.6 wt% of hydrogen with respect to the $LiAlH_4$ under 385–493 K and 400–533 K, respectively, creating a total theoretical hydrogen capacity of 7.9 wt%. The hydrogen release temperature rises to 673 K for the third reaction due to the high stability of the LiH, which is too high for practical purposes.[12] The reactions (1)–(3) are characterized by very slow kinetics and reversibility occurs only under severe conditions. The hydrogen desorption kinetics have been improved by milling $LiAlH_4$ with additives[5–7,13,14] and some degree of reversibility (1.8 wt%) was achieved by Chen *et al.*[14] In addition, Liu *et al.* demonstrated that reversibility can be up to 7 wt% at Ti-doped $LiAlH_4$.[15] Mao *et al.* found that TiF_3 exhibited superior catalytic effect on the hydriding/dehydriding kinetics of the $LiAlH_4$–$LiBH_4$ system.[16] Beattie *et al.* using scanning electron microscope (SEM) observed the dehydrogenation processes of $LiAlH_4$ at the sub-micron level, and found there is little or no morphological structural changes associated with heating.[17] However, at present, neither the mechanism of absorption and desorption of hydrogen nor the role of additives are well understood.

The use of Ti- and Fe-based catalysts increases the rate of the mechanochemical transformation of $LiAlH_4$ into Li_3AlH_6, Al and H_2.[6] The degree of the catalytic effect decreases in the order of $TiCl_4$ > Al_3Ti > $Al_{22}Fe_3Ti_8$ > Al_3Fe > Fe. Recently Kojima *et al.* studied the mechanochemical reactions of $LiAlH_4$ catalyzed with the transition metal chlorides $TiCl_3$, VCl_3, $NiCl_2$, $ZnCl_2$, and $ZrCl_4$[18] and found that doping with $TiCl_3$ and $ZrCl_4$ eliminates reactions (1) and (2), whereas doping with other catalysts only eliminates reaction (1). Naik *et al.*[19] reported the dehydrogenation properties of $LiAlH_4$ wet-doped with Sc, Ti, or V transition metals, and found the transition metals could decrease the decomposition temperature down to 303–313 K. The catalytic activity increases in the order of V, Ti to Sc.[19]

First-principles calculations have also been used to investigate the structures,[20] thermodynamics and phase diagram, and the

[a] *School of Materials Science and Engineering, Harbin Institute of Technology at Weihai, 2 West Wenhua Road, Weihai, 264209, China. E-mail: sy@hitwh.edu.cn*
[b] *Institute of Metal Research, Chinese Academy of Sciences, 72 Wenhua Road, Shenyang 110016, China*

stability and decompositions of lithium alanate.[21,22] Løvvik *et al.* used the harmonic phonon approximation and first-principles calculations to find that the calculated reaction enthalpy for reaction (1) is positive, suggesting that this reaction is endothermic.[23] Frankcombe and Kroes used the same approaches to find that the decomposition of $LiAlH_4$ is spontaneous even at low temperature.[24]

The enthalpy of formation for $LiAlH_4$ at 298 K was reported to be -113.42 kJ mol^{-1} after applying vibrational corrections to the cohesive energy in the DFT calculations.[23] Monte Carlo simulations of isolated and solvated $LiAlH_4$ have also been used to investigate its structural changes when it is in solution or in a vacuum.[25] The $LiAlH_4$ and its dimer $[LiAlH_4]_2$ were characterized in vacuum and in a dimethyl ether solution using Hartree–Fock (HF), Møller–Plesset (MP2), and DFT electronic structure calculations coupled with the polarized continuum solvation model (PCM) to describe the structural properties of $LiAlH_4$ at a finite temperature.[26] The bidentate isomer was found to be in greater concentration in both vacuum and solution simulations at 300 K, as predicted by the PCM calculations. The stability of the low-index surfaces (001), (010), (100) and (101) of crystalline $LiAlH_4$ has been studied by performing periodic density functional calculations within the generalized gradient approximation.[27] Surface energy calculations have shown that the most stable surfaces consist of Li, Al, and a mixture of these atoms.

Although many studies have centralized on the dehydrogenation properties of $LiAlH_4$, the catalytic mechanisms of transition metals are still poorly understood. We have applied a first-principles method to investigate the mechanisms of Ti and Ni influence on the dehydrogenation properties of $NaAlH_4$, and found that the two dopants use different mechanisms to improve the dehydrogenation properties of the $NaAlH_4$. The Ti may generate a TiH_2 phase if it occupies an interstitial site or form Ti–Al intermetallics if it replaces an Al atom, resulting in greatly improved dehydrogenation properties. While the influence of Ni on the dehydrogenation properties of $NaAlH_4$ is relatively weak when compared to the Ti dopant, largely because Ni only affects the electronic distribution in its vicinity, this is not the case for the stability of the $[AlH_4]$ groups.[28,29] In this paper, we applied first-principles calculations to investigate the mechanisms of the influence of dopants Ti and Ni on the dehydrogenation properties of $LiAlH_4$.

Methodology

The electronic structure and the total energy of pure and M (M = Ti or Ni) doped $LiAlH_4$ were calculated by VASP code (version 4.6.9)[30,31] using the generalized gradient approximation of Perdew and Wang.[32] The project augmented wave method was used to span out the valence electron density.[33] A cut-off energy of 450 eV and a Gaussian smearing method with an energy broadening of 0.2 eV were used throughout. The criterion for self-consistency when determining the electronic structure was that two consecutive energies differed by less than 0.01 meV. The accuracy of the total energy on the k-mesh was checked for $4 \times 3 \times 3$ and $8 \times 6 \times 6$ k-meshes, and, as the difference in the total energy of the two processes was less than 0.001 eV, the $4 \times 3 \times 3$ k-mesh was used.

Results and discussions

1 Occupation energy

The structure of $LiAlH_4$ was determined from powder X-ray and neutron diffraction analysis at both 295 K and 8 K.[34] The symmetry group of $LiAlH_4$ is $P2_1/c$ (no. 14) and the lattice parameters are $a = 0.48174(1)$, $b = 0.78020(1)$, $c = 0.78214(1)$ nm, $\alpha = 90^\circ$, $\beta = 112.228^\circ$, and $\gamma = 90^\circ$.[34] In order to check the accuracy of the calculations, a full relaxation for the unit cell was performed and the atomic coordinates and both the size and shape of the cell of the pure $LiAlH_4$ were measured. The calculated lattice parameters and the atomic coordinates are listed in Table 1. The experimental values of the lattice parameters are listed alongside the calculated values and show reasonable agreement. The heat of formation of $LiAlH_4$ was estimated as -118.41 kJ mol^{-1}, close to the experimental value of -119.32 kJ mol^{-1} at 298 K,[35] another theoretical calculation of -113.42 kJ mol^{-1} [23] and our previous full potential calculation of -105.56 kJ mol^{-1}.[22] To estimate the reaction enthalpy of reaction (1), the ground state energies of the Li_3AlH_6, $Im\bar{3}m$ Li metal, $Fm\bar{3}m$ Al and the diatomic H_2 gas were calculated. The total energies of the dopants, $Fm\bar{3}m$ Ni and $P6_3/mmc$ Ti metals were also calculated. Experimental values were used for the bulk lattice constants of these elements and the H_2 gas was simulated using a $1 \times 1 \times 1$ nm^3 cell. The calculated enthalpy of reaction (1) is 9.52 kJ mol^{-1} H_2, close to another theoretical calculation of 9.79 kJ mol^{-1} H_2.[23] The predicted endothermic reaction of reaction (1) agrees with a recent experimental observation.[36]

In the present work, we first used $2 \times 1 \times 1$ and $2 \times 1 \times 2$ supercells to investigate the influence of dopants on the dehydrogenation properties of $LiAlH_4$. After full relaxations, geometric structures and the formation energies of the considered systems obtained from the two supercells were very close. For example, the largest difference in the bond length between the Ti and its surrounding atoms is about 4%. Therefore, only the $2 \times 1 \times 1$ supercell containing eight $LiAlH_4$ cells was used in the present work (Fig. 1). The M-doped system (where M is Ti or Ni) is denoted as $(Li_{8-x}Al_{8-y}M_{x+y+z})H_{32}$, where ($x = 1$, $y = 0$, $z = 0$) and ($x = 0$, $y = 1$, $z = 0$) refer to the M substitution for the Li and Al site, respectively, and ($x = 0$, $y = 0$, $z = 1$) means M occupies an interstitial site. (0.5302, 0.4656, 0.8266) was chosen as the initial coordinates of the interstitial site and a full relaxation of each doped system was performed. The stability of each doped system can be described by the difference in total energy between that doped system and both the un-doped $LiAlH_4$ and the pure metal reference systems. We therefore define the occupation energy in eqn (4) using E(M) for the total energy of system M:

$$E_{occu} = E(Li_{8-x}Al_{8-y}M_{x+y+z}H_{32}) - E(Li_8Al_8H_{32}) - \{(x+y+z)E(M) - xE(Li) - yE(Al)\} \quad (4)$$

The calculated total energy, the lattice parameters, the coordinates of dopant and occupation energy of the considered

Table 1 The calculated and experimental lattice parameters of the $LiAlH_4$

	Lattice parameters/nm		Coordinates					
			Present			Expt.[25]		
	Present	Expt.[25]	*x*	*y*	*z*	*x*	*y*	*z*
a	0.47878	0.48174	—			—		
b	0.77428	0.78020	—			—		
c	0.77171	0.78214	—			—		
β	111.895°	112.228°	—			—		
Li	—	—	0.5754	0.4624	0.8266	0.5603	0.4656	0.8266
Al	—	—	0.1462	0.2040	0.9333	0.1386	0.2033	0.9302
H1	—	—	0.1872	0.0988	0.7635	0.1826	0.0958	0.7630
H2	—	—	0.3628	0.3745	0.9794	0.3524	0.3713	0.9749
H3	—	—	0.2461	0.0835	0.1167	0.2425	0.0806	0.1148
H4	—	—	0.8022	0.2661	0.8730	0.7994	0.2649	0.8724

systems are listed in Table 2. In general, the dopant, M, shrinks the lattice of the $LiAlH_4$ in the *b* direction. The configurations in which the Ti or Ni dopant occupies the interstitial site have the lowest occupation energy among the systems that were considered here, and the lowest value was obtained when Ni occupied the interstitial site. The occupational behavior of Ti and Ni in $LiAlH_4$ is not the same as in $NaAlH_4$; although the dopants still prefer to occupy interstitial sites, in the $NaAlH_4$ the Ti has the lowest occupation energy if it substitutes for an Al atom.[28]

The Ti and Ni are least likely to substitute for either the Al or Li atoms due to the higher occupation energies required. As a result, the following sections only analyse the bonding characteristics between the Al and the H atoms within an $[AlH_4]$ group and the electronic structures for the un-doped and the interstitially occupied $LiAlH_4$ systems.

2 Bonding interactions

The estimation of bonding interaction between atoms in a compound is challenging. Both binding energy (defined as the difference between the total energy of a system and the sum of the energies of individual atoms, averaged over the number of atoms in the system) and cohesive energy are usually used as a measurement of the interaction between atoms. We chose the individual atoms as a reference when calculating the binding energy and the metals or molecules in each system when estimating the cohesive energy. A previous study on the ternary MgH_2 systems has shown that the vibration of H atoms around their equilibrium positions is almost harmonic.[37] This shows us how to investigate the bonding mechanism between the H atom and the matrix atoms. We propose here a model that gives an estimation of the interaction energies between a specific atom (or ligand) X and the matrix in $LiAlH_4$. In this model, one H atom is vibrating around its equilibrium position in the H–host bond direction while other atoms in this system are kept at their equilibrium positions so that the curve of total energy against bond length of the H–host bond can be evaluated. In this paper the bonding interactions between the H*x* (x = 1 to 4) and the host Al atoms in the $[AlH_4]$ group nearest to the dopants are estimated using this model. The estimated curves of the total energy against the Al–H*x* bond length for the Al–H*x* (x = 1 to 4) bonds in $LiAlH_4$ systems with and without dopant are plotted in Fig. 2. The H atoms in the un-doped $LiAlH_4$ system interact almost equally with the Al atom resulting in similar bond strengths (the shape of the energy–bond length curve) and bond lengths (with the exception of the Al–H2 bond in Fig. 2(a), which has a slightly longer bond length). However, the energy–bond length curves of the doped $LiAlH_4$ systems were dramatically different to those of the un-doped system (Fig. 2(b) and (c)), revealing the significant influence the dopants have on the stability of their neighbouring $[AlH_4]$ group and the interactions between atoms within this group. In the Ti-doped $LiAlH_4$ system, the Al–H*x* (x = 1, 2, or 4) bonds were stretched, while the Al–H3 bond remained almost unchanged, whereas in the Ni-doped system, the Al–H*x* (x = 1, 2, or 3) bonds were stretched while the Al–H4 bond remained almost unchanged. In both the Ti- and the Ni-doped systems the Al–H1 bond was the longest.

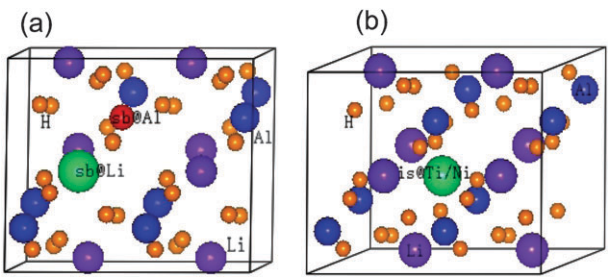

Fig. 1 Supercells employed in this work. The Al, the Li, and the H atoms were denoted as the medium blue, the medium violet, and the small gold balls, respectively, as labeled. (a) Dopant M substitutes for an Al atom (the second small and red ball) and for a Li atom (the largest and green ball), respectively, and (b) dopant M occupies an interstitial site (the large green ball).

To compare the three systems on the same scale we defined the bonding energy as given below, using $E_{tot}(M)$ to denote the total energy of system M and $E'_{tot}(M)$ as the total energy of the system M with a H atom removed:

$$E_b = E_{tot}(M) - \left[E'_{tot}(M) + \frac{1}{2}E_{tot}(H_2)\right] \qquad (5)$$

Using this definition, Fig. 2 was re-plotted as the E_b against the bond length in Fig. 3. The curves in Fig. 3 are parabolic or nearly parabolic and so have been fitted using the function below, in which r_0 is the bond length, k_1 is a bond strength

Table 2 Lattice parameters (nm), positions, and total and occupation energies (in eV) of dopants in the M doped-$LiAlH_4$ systems

				Lattice parameter/nm			M coordinates				
M	x	y	z	a	b	c	u	v	w	$E(Li_{8-x}Al_{8-y}M_{x+y+z}H_{32})$	E_{occu}
—	0	0	0	0.4788	0.7743	0.7717	—	—	—	−163.008	0
Ti	1	0	0	0.4657	0.7322	0.7871	0.2459	0.5344	0.7923	−166.890	1.983
	0	1	0	0.4826	0.7599	0.7554	0.4537	0.6679	0.5280	−165.522	1.497
	0	0	1	0.4610	0.7362	0.7759	0.5742	0.5385	0.8352	−170.149	0.591
Ni	1	0	0	0.4793	0.7751	0.7464	0.2988	0.4628	0.8642	−164.178	2.329
	0	1	0	0.4596	0.7307	0.7958	0.5046	0.6332	0.6040	−162.753	2.044
	0	0	1	0.4751	0.7454	0.7737	0.5229	0.4111	0.7514	−168.345	0.144

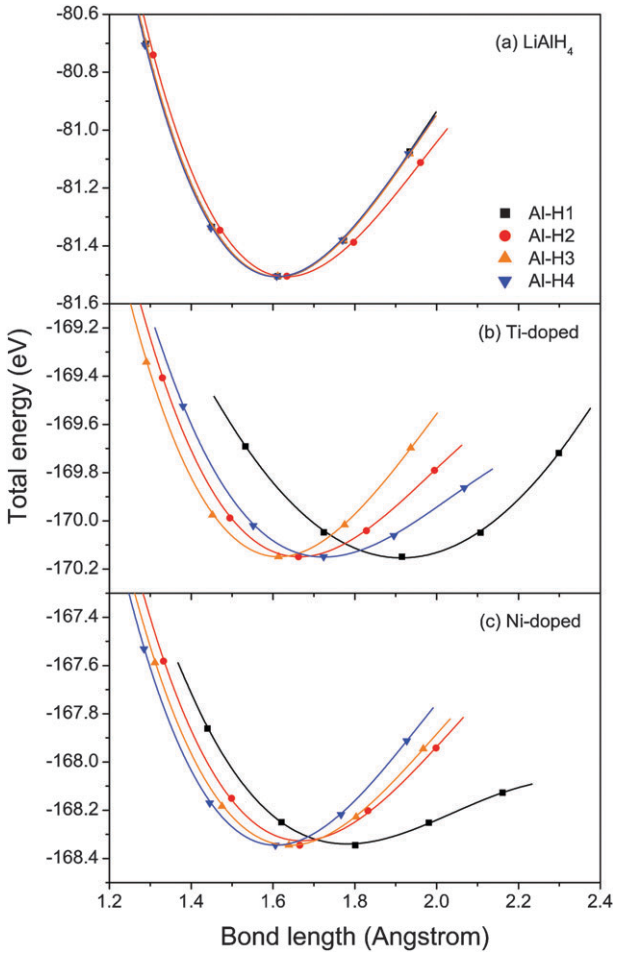

Fig. 2 Curves of the total energies against the Al–H bond lengths for (a) the un-doped, (b) the Ti-doped, and (c) the Ni-doped $LiAlH_4$ systems.

parameter and k_2 describes the contributions of the non-harmonic interactions to the bond energy:

$$E_b = E_0 + \tfrac{1}{2}k_1(r - r_0)^2 + \tfrac{1}{6}k_2(r - r_0)^3 \qquad (6)$$

The values of these parameters fitted from the Fig. 3 are listed in Table 3. In the un-doped $LiAlH_4$ the Al–H2 bond is the weakest, with a bond energy of 1.71 eV, a bond length of 0.163 nm and a bond strength parameter k_1 = 10.9 eV Å^{-2}, while the Al–Hx (x = 1, 3, or 4) bonds are almost the same, with a bond energy of 1.75–1.78 eV, a bond length around 0.161 nm, and a k_1 value of around 11.9 eV Å^{-2}. These findings are consistent with previous full potential calculations that show the H2 atom as a bridge connecting the Li ion and the [AlH_4] group.[22]

The activation energy for reaction (1) using a low heating rate was reported experimentally as around 160 kJ mol^{-1}.[36,38] In general, the decomposition of a compound starts with the breaking of the weakest bond (the Al–H2 bond in the $LiAlH_4$ system, which requires at least 1.71 eV = 164.98 kJ mol^{-1} of energy). Due to the complexity of a reaction, the predicted bond energy and the reaction activation energy are not directly connected, but the agreement of theoretical bond energy and the experimental activation energy provides evidence that the

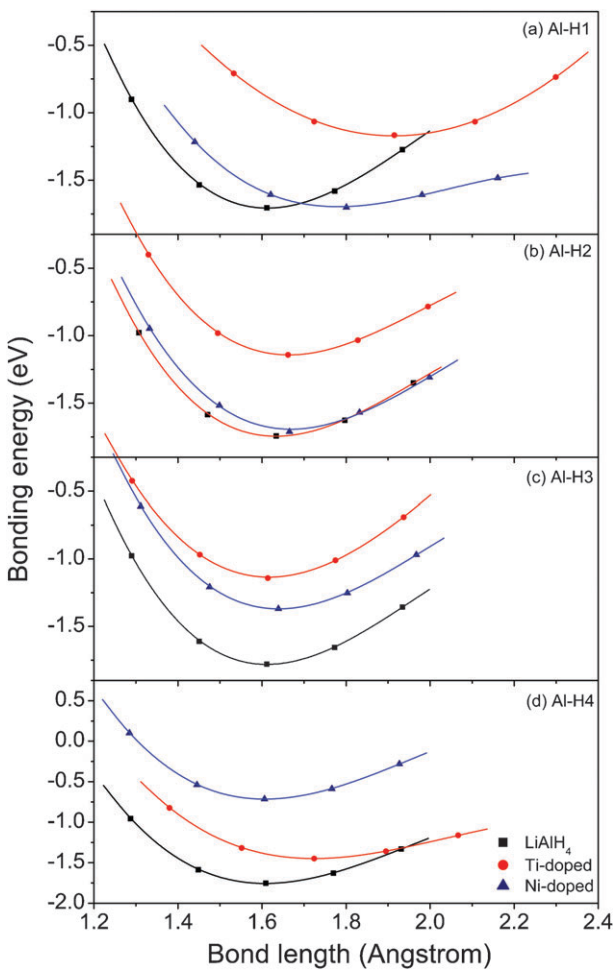

Fig. 3 Curves of the bond energy against the Al–Hx (x = 1 to 4) bond lengths.

Table 3 Bonding parameters fitted from the calculated energy-bond length curves estimated for the pure and doped $LiAlH_4$ systems

Bond	E_0/eV	r_0/Å	k_1/eV Å^{-2}	k_2/eV Å^{-3}
Al–H1	−1.748	1.612	10.98	−33.07 ($LiAlH_4$)
	−1.173	1.914	6.13	−1.94 (Ti_inter)
	−1.698	1.780	5.80	−22.28 (Ni_inter)
Al–H2	−1.709	1.632	11.96	−33.07 ($LiAlH_4$)
	−1.145	1.663	9.97	−31.02 (Ti_inter)
	−1.695	1.668	10.21	−27.91 (Ni_inter)
Al–H3	−1.784	1.611	11.88	−34.39 ($LiAlH_4$)
	−1.138	1.616	11.08	−22.67 (Ti_inter)
	−1.373	1.639	10.82	−30.65 (Ni_inter)
Al–H4	−1.758	1.608	11.93	−34.88 ($LiAlH_4$)
	−1.451	1.723	7.77	−25.23 (Ti_inter)
	−0.717	1.606	12.14	−34.47 (Ni_inter)

proposed model is a reasonable description of the bonding interactions.

All the Al–H bonds were significantly weaker in the Ti-doped $LiAlH_4$ than in the un-doped $LiAlH_4$, with the k_1 values between 6.13 to 11.08 eV Å^{-2}. The bond lengths of the Al–H bonds were stretched to different degrees, the longest of which are the Al–H1 bonds (r_0 = 0.1914 nm from Table 3) in the Ti-doped $LiAlH_4$. This distorted the geometry of the $[AlH_4]$ group, reducing its stability. Similar results can be found in the Ni-doped $LiAlH_4$, whose weakest bond is the Al–H1 bond with a bond length of 0.178 nm and a k_1 value of 5.80 eV Å^{-2}. The catalytic effect of Ti in $LiAlH_4$ is greater than that of Ni as Ti produces a larger overall reduction in k_1 values and stretches the Al–H bonds further, distorting the $[AlH_4]$ group more than the Ni dopant.

3 Electronic structures

The total and partial densities of states (DOS) for the considered systems were calculated and are plotted in Fig. 4–6. Fig. 4 shows the total and partial DOSs of the un-doped $LiAlH_4$ system. The total DOS shows a 4.5 eV energy gap between the valence and the bottom conduction bands. The valence electrons are distributed in two energy ranges; from −6.0 to −4.0 eV and from −3.0 eV to the Fermi energy level. The upper range (the main body of the interactions between atoms) is created by the H s and the Li p and Al p electrons and the lower range is the result of the s electron interactions. In the partial DOSs of Li atom, the bonding peaks appear in the energy range from −6.0 to −4.0 eV and from −3.0 eV to the Fermi energy level. The main contributions to the antibonding peaks in the total DOS are the antibonding states of Li, which are located in the energy range from 4.5–8.0 eV. This means covalent bonding characteristics dominate the interaction between the Li cation and the $[AlH_4]^{-1}$ ion. The observation that the bonding peaks are much higher than the antibonding peaks for the Al and H atoms of the $[AlH_4]$ group is an ionic feature. The partial DOSs of the H1, H3 and H4 atoms show similar distributions, but the amplitude of the H2 partial DOS in the upper energy range is lower than that of the other three H atoms, implying a weak bonding between Al and H2 within the $[AlH_4]$ group.

Fig. 5 is the total and partial DOSs of the Ti-doped $LiAlH_4$. The band gap between the bonding and the antibonding states

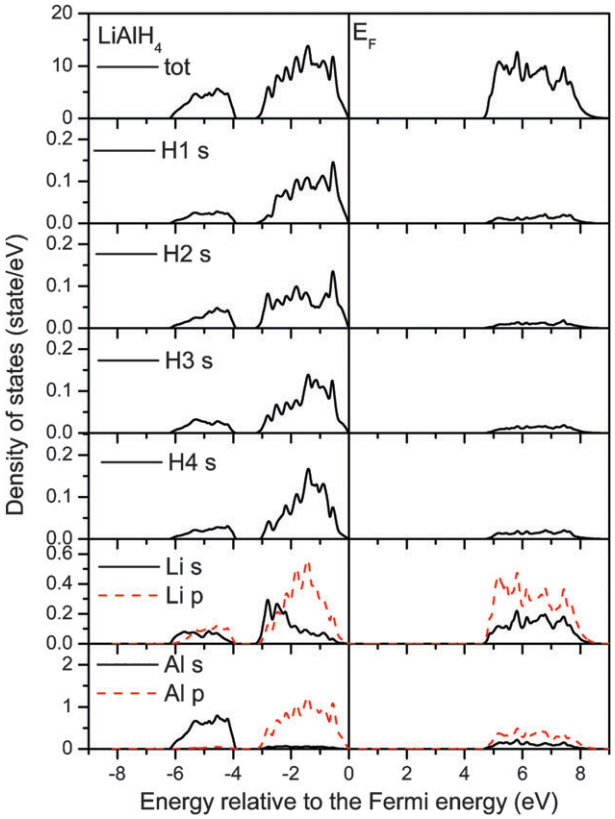

Fig. 4 Total and partial densities of states for the un-doped $LiAlH_4$ system.

is only 1.5 eV, and the Ti d, Al p, and some H s electrons contribute to new bonding peaks in the energy range from −1.0 eV to the Fermi energy level of the total DOS. The Ti interacts with the Al atom in the Ti-doped $LiAlH_4$ by increasing the amplitude of the Al p and s electrons in this energy region, and may also attract the H3 and the H4 atoms as both the partial DOSs of H3 and H4 s electrons show a bonding peak in this energy region. This is similar to the interactions in Ti-doped $NaAlH_4$, where the Ti uses 'captured' H atoms to form the TiH_2 phase or interacts with the Al atom to help form Ti–Al intermetallics.[28] Stronger bonding peaks at around −5.0 eV can be identified between the Al and the H2, H3 and H4 atoms in the $[AlH_4]$ group. The region near −3.0 eV contains the main bonding peak of the H1 atom yet relatively few Al p electrons, implying a relatively weak interaction between the Al and the H1 atoms. The partial DOS of the H1 atom also shows that there are no bonding peaks in the energy range from −2.0 eV to the Fermi energy level, so the H1 atom may easily be released during the dissociation of the Ti-doped $LiAlH_4$. The main bonding distributions (the upper region of its partial DOS, from about 3.0 eV in pure $LiAlH_4$ and about 4.0 eV in the Ti-doped $LiAlH_4$) of the Li p and s electrons were broadened and shifted about 2.0 eV toward the lower energy range. The greatest influence the Ti dopant has on the stability and bonding interactions of the $LiAlH_4$ compound occurs when the Ti d electrons located at −1.0 eV below the Fermi energy interact with the Al p and s electrons in the same energy range, 'freeing' the H1 and H2 atoms from the Al atoms.

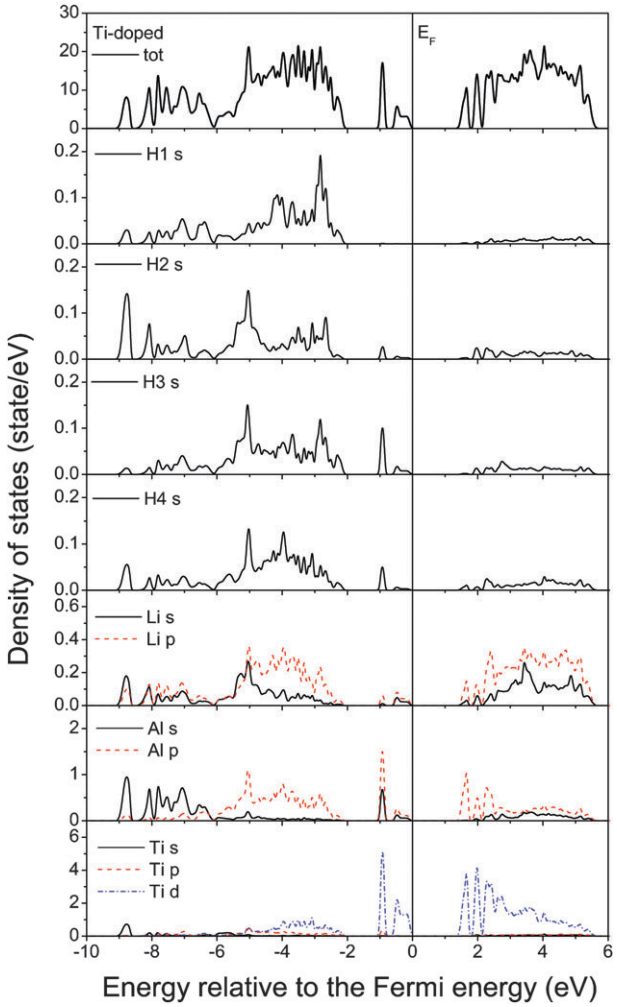

Fig. 5 Total and partial densities of states for the Ti-doped $LiAlH_4$ system.

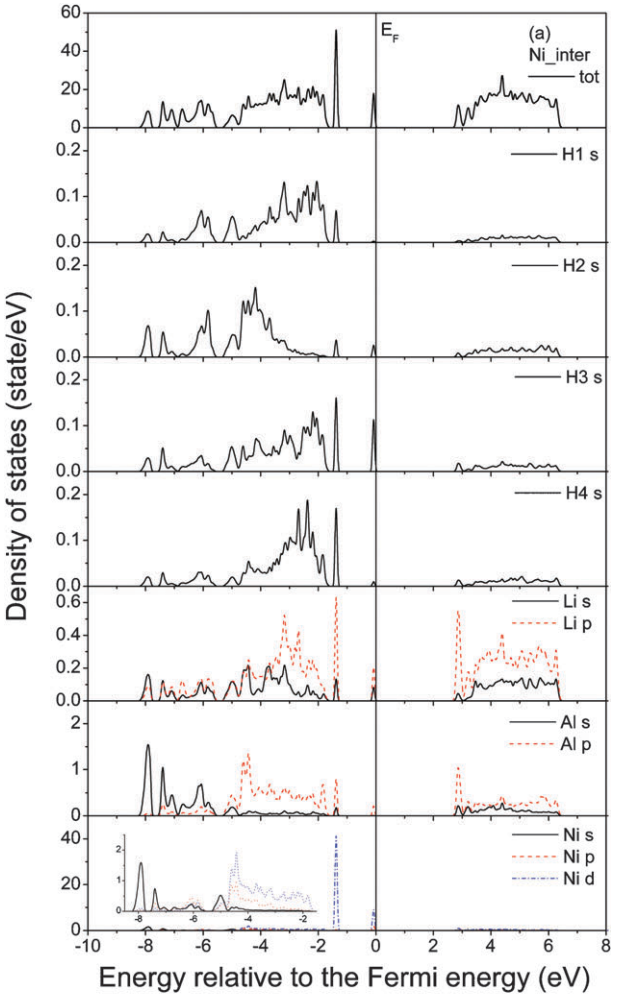

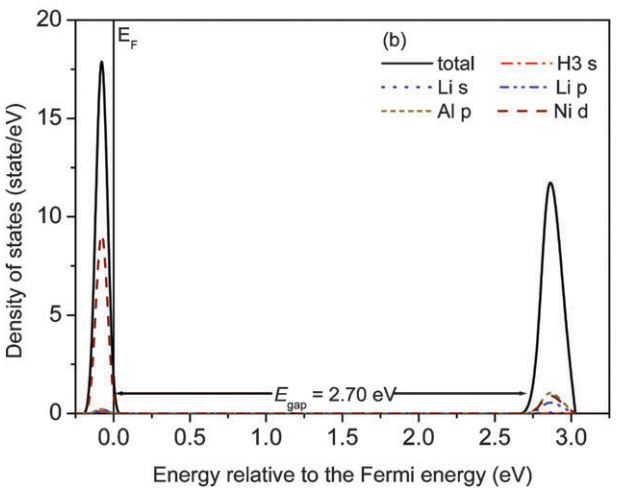

Fig. 6 Total and partial densities of states for the Ni-doped $LiAlH_4$ system (a) and an enlargement of the bond gap (b).

The total and partial DOSs of the Ni-doped $LiAlH_4$ are shown in Fig. 6. The Ni induces a sharp bonding peak dominated by the Ni d, Al p, Li p, H3 s, and H4 s electrons at −1.5 eV below the Fermi energy in the total DOS of this system. The Ni–Al interaction usually forms the Ni–Al compound, whereas the Li–H interactions cause the formation of the LiH phase. The partial DOSs of the Al and the H atoms in Fig. 6 indicate that these two interactions will reduce the stability of the $[AlH_4]$ group. The Al p electrons that are distributed in the energy range from −5.5 to −1.8 eV and have a peak at about −4.5 eV dominate the Al–H bonding interactions. This, together with the observation that the H2 s electrons peaks are also in this energy range, implies that the Al–H2 bond is the strongest within the $[AlH_4]$ group. Similarly, the weaker electron distributions in this energy range for the H1, H3, and H4 atoms imply weaker interactions between these H atoms and the Al. These results combined with Table 3 and Fig. 2 and 3 show that the Al–H1 bond is the weakest bond in this system and the H1 atom will be released first if this system is decomposed. The influence the dopant Ni has on the stability and the bonding interactions of the $LiAlH_4$ comes from the bonding interaction between the Ni and the Al caused by the introduction of the Ni d electrons. This interaction strengthens the interactions between the Li and its neighbouring H atoms, which may cause a formation of a LiH phase that, in turn, may 'free' the H1 and H2 atoms from the $[AlH_4]$ group.

The charge difference densities (CDD) of the pure and the Ti/Ni doped $LiAlH_4$ systems are plotted in Fig. 7 and 8 to

further illustrate the electronic structures and bonding characteristics of the considered systems. The CDD is defined below using ρ_{sys} to denote the charge distribution of the considered system and ρ_i^{atom} to denote the charge distribution of the individual atoms that make up the system:

$$\rho_{CDD} = \rho_{sys} - \sum_i \rho_i^{atom} \quad (7)$$

Fig. 7(a) shows a top-down view of the three dimension CDD on the (001) plane, with the positive CCD coloured blue and the negative red. Fig. 7(b) is the projection of the three dimensional CDD on the (001) plane, and uses solid and dashed lines to denote the positive and the negative CDD. The interactions between the Al and the H atoms in Fig. 7(b) are clearly ionic in nature and the Al atom almost equally interacts with the H atoms; these interactions trace an equilateral triangle with the three H atoms in the corners and the Al atom at the centre.

The CDD of the (001) plane of the Ti-doped $LiAlH_4$ system in Fig. 8(a) shows the distortion of the [AlH_4] groups around the Ti atom and a dramatic reduction of the CDD around the H1 atom that causes a weakened bonding between the Al and the H1 atoms; both of which increase the amount of hydrogen released by the system. The CDD of the (001) plane of the Ni-doped $LiAlH_4$ system in Fig. 8(b) shows that the H1 atoms have moved away from the Al atoms and that the Al–H triangles were distorted.

It should be pointed out that the low CDD around the Li atoms (Fig. 7(a)) makes it hard to trace the Li atoms in the projection of the CDD on the (001) plane for the systems considered here (Fig. 7(a), 8(a) and (b)).

Conclusions

We used first-principles calculations to study Ti- and Ni-doped $LiAlH_4$ systems. The results show that both the Ti and Ni prefer to occupy an interstitial site with relatively small occupation energies of 0.591 and 0.144 eV, respectively. The geometry and the stability of the [AlH_4] group are distorted in the doped $LiAlH_4$ systems, and the bonding interactions between its Al and H atoms are dramatically reduced too. The electronic structure analysis shows that the bonding between the Al and the H atoms in the [AlH_4] group is ionic in nature, yet the bonding between the Li atom and the [AlH_4] group is covalent. The influence of the dopant Ti on the stability and bonding interactions of the $LiAlH_4$ comes from the interactions of the Ti d electrons with the Al atom in their neighbouring [AlH_4] groups and the 'freeing' of the H1 and H2 atoms from these [AlH_4] groups. The Ni dopant affects the stability and bonding interactions of the $LiAlH_4$ by introducing Ni d electrons that cause a bonding interaction between the Ni and the Al, 'freeing' the H1 and H2 atoms from the [AlH_4] group and strengthening the interactions between the Li and its neighbouring H atoms so that they sometimes form LiH phases.

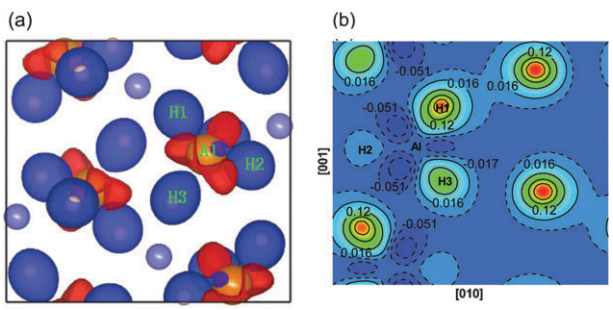

Fig. 7 Charge difference distribution in the un-doped $LiAlH_4$ system. (a) The top-down view of the three dimensional CDD on the (001) plane, and (b) the projection of the CDD on the (001) plane.

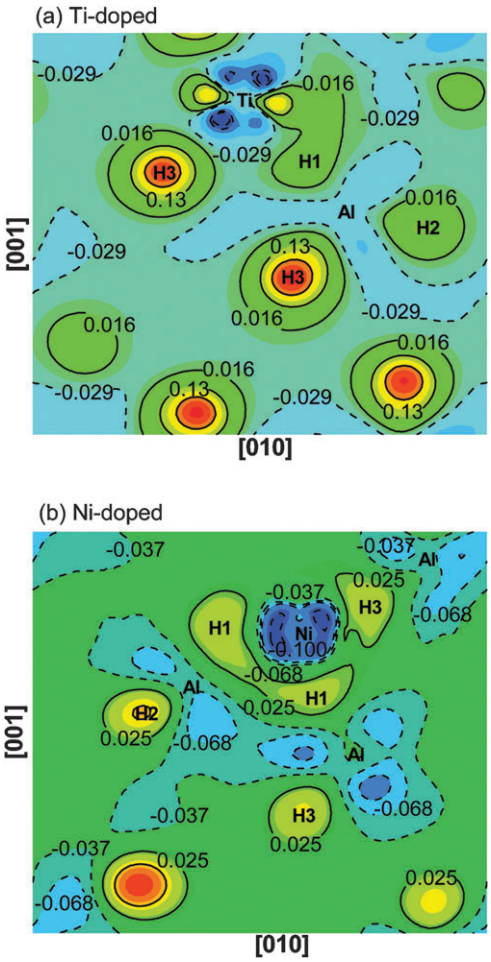

Fig. 8 Charge difference distribution on the (001) plane for (a) the Ti-doped and (b) the Ni-doped $LiAlH_4$ system, respectively.

Acknowledgements

This work was supported by the National Basic Research Programme of China Grant 2006CB605104, the Natural Science Foundation of Shandong Province (Y2007F61), and the Programme of the Excellent Team of Harbin Institute of Technology.

References

1 J. Graetz and J. J. Reilly, *Scr. Mater.*, 2007, **56**, 835.
2 A. R. Akbarzadeh, C. Wolverton and V. Ozolins, *Phys. Rev. B: Condens. Matter Mater. Phys.*, 2009, **79**, 184102.

3 H. Grove, H. W. Brinks, R. H. Heyn, F.-J. Wu, S. M. Opalka, X. Tang, B. L. Laube and B. C. Hauback, *J. Alloys Compd.*, 2008, **455**, 249.
4 B. Bogdanović and M. Schwickardi, *J. Alloys Compd.*, 1997, **253–254**, 1; B. Bogdanović, U. berle, M. Felderhoff and F. Schüth, *Scr. Mater.*, 2007, **56**, 813.
5 V. P. Balema, V. K. Pecharsky and K. W. Dennis, *J. Alloys Compd.*, 2000, **313**, 69.
6 V. P. Balema, J. W. Wiench, K. W. Dennis, M. Pruski and V. K. Pecharsky, *J. Alloys Compd.*, 2001, **329**, 108.
7 M. Resan, M. D. Hampton, J. K. Lomness and D. K. Slattery, *Int. J. Hydrogen Energy*, 2005, **30**, 1413.
8 W. E. Garner and E. W. Haycock, *Proc. R. Soc. London, Ser. A*, 1952, **211**, 335.
9 J. Block and A. P. Gray, *Inorg. Chem.*, 1965, **4**, 304.
10 J. A. Dilts and E. C. Ashby, *Inorg. Chem.*, 1972, **11**, 1230.
11 J. P. Bastide, B. Bonnetot, J. M. Letoffe and P. Claudy, *Mater. Scr. Bull.*, 1985, **20**, 997.
12 D. Blanchard, H. W. Brinks, B. C. Hauback and P. Norby, *Mater. Sci. Eng., B*, 2004, **108**, 54.
13 M. Resan, M. D. Hampton, J. K. Lomness and D. K. Slattery, *Int. J. Hydrogen Energy*, 2005, **30**, 1417.
14 J. Chen, N. Kuriyama, Q. Xu, H. T. Takeshita and T. Sakai, *J. Phys. Chem. B*, 2001, **105**, 11214.
15 X. F. Liu, G. S. McGrady, H. W. Langmi and C. M. Jensen, *J. Am. Chem. Soc.*, 2009, **131**, 5032.
16 J. F. Mao, Z. P. Guoa, H. K. Liu and X. B. Yu, *J. Alloys Compd.*, 2009, **487**, 434.
17 S. D. Beattie and G. S. McGrady, *Int. J. Hydrogen Energy*, 2009, **34**, 9151.
18 Y. Kojima, Y. Kawai, M. Matsumoto and T. Haga, *J. Alloys Compd.*, 2008, **462**, 275.
19 M. Naik, S. Rather, C. S. So, S. W. Hwang, A. R. Kim and K. S. Nahm, *Int. J. Hydrogen Energy*, 2009, **34**, 8937.
20 P. Vajeeston, P. Ravindran, R. Vidya, H. Fjellvag and A. Kjekshus, *Phys. Rev. B: Condens. Matter Mater. Phys.*, 2003, **68**, 212101.
21 X. Ke and C. F. Chen, *Phys. Rev. B: Condens. Matter Mater. Phys.*, 2007, **76**, 024112.
22 Y. Song, R. Singh and Z. X. Guo, *J. Phys. Chem. B*, 2006, **110**, 6906.
23 O. M. Løvvik, S. M. Opalka, H. W. Brinks and B. C. Hauback, *Phys. Rev. B: Condens. Matter Mater. Phys.*, 2004, **69**, 134117.
24 T. J. Frankcombe and G.-J. Kroes, *Phys. Rev. B: Condens. Matter Mater. Phys.*, 2006, **73**, 174302.
25 E. Asciutto, A. Crespo and D. A. Estrin, *Chem. Phys. Lett.*, 2002, **353**, 178.
26 M. Cossi, V. V. Barone, R. Cammi and J. Tomasi, *Chem. Phys. Lett.*, 1996, **255**, 327.
27 O. M. Løvvik, *J. Alloys Compd.*, 2003, **356–357**, 178.
28 Y. Song, J. H. Dai, C. G. Li and R. Yang, *J. Phys. Chem. C*, 2009, **113**, 10215.
29 J. H. Dai, C. G. Li and Y. Song, *Acta Chimica Sinica.*, 2009, **67**, 1447.
30 G. Kresse and J. Hafner, *Phys. Rev. B: Condens. Matter*, 1993, **47**, 558.
31 G. Kresse and J. Furthmüller, *Phys. Rev. B: Condens. Matter*, 1996, **54**, 11169.
32 J. P. Perdew, J. A. Chevary, S. H. Vosko, K. A. Jackson, M. R. Pederson, D. J. Singh and C. Fiolhais, *Phys. Rev. B: Condens. Matter*, 1992, **46**, 6671.
33 G. Kresse and D. Joubert, *Phys. Rev. B: Condens. Matter Mater. Phys.*, 1999, **59**, 1758.
34 B. C. Hauback, H. W. Brinks and H. Fjellvag, *J. Alloys Compd.*, 2002, **346**, 184.
35 M. B. Smith and G. E. Bass, *J. Chem. Eng. Data*, 1963, **8**, 342.
36 J. R. Ares, K. -F. Aguey-Zinsou, M. Porcu, J. M. Sykes, M. Dornheim, T. Lassen and R. Bormann, *Mater. Res. Bull.*, 2008, **43**, 1263.
37 Y. Song and R. Yang, *Int. J. Hydrogen Energy*, 2009, **34**, 3778.
38 J. K. Kang, J. K. Lee, R. P. Muller and W. A. Goddard, *J. Chem. Phys.*, 2004, **121**, 10623.